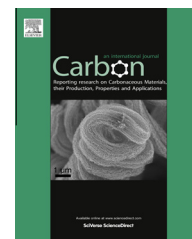


Available at [www.sciencedirect.com](http://www.sciencedirect.com)

ScienceDirect

journal homepage: [www.elsevier.com/locate/carbon](http://www.elsevier.com/locate/carbon)

# Controllable bulk growth of few-layer graphene/single-walled carbon nanotube hybrids containing Fe@C nanoparticles in a fluidized bed reactor

Meng-Qiang Zhao, Hong-Jie Peng, Qiang Zhang\*, Jia-Qi Huang, Gui-Li Tian, Cheng Tang, Ling Hu, Hai-Rong Jiang, Hong-Ying Cai, Hong-Xia Yuan, Fei Wei

Beijing Key Laboratory of Green Chemical Reaction Engineering and Technology, Department of Chemical Engineering, Tsinghua University, Beijing 100084, China

## ARTICLE INFO

Article history:

Received 22 August 2013

Accepted 11 October 2013

Available online 19 October 2013

## ABSTRACT

A family of layered double hydroxides (LDHs) with varied Fe contents were employed as catalyst precursors for the controllable bulk growth of few-layer graphene/single-walled carbon nanotube (G/SWCNT) hybrids in a fluidized-bed reactor through chemical vapor deposition of methane at 950 °C. All the G/SWCNT hybrids exhibited the morphology of SWCNTs interlinked with graphene layers. The purity, thermal stability, graphitization degree, specific surface area, and total pore volume of the G/SWCNT hybrids decreased with the increasing Fe contents in the LDH precursors. A high yield of 0.97 g<sub>G/SWCNTs</sub>/g<sub>cat</sub> can be achieved by tuning the Fe content in the FeMgAl LDHs after a 15-min growth. After the removal of the as-calcined FeMgAl layered double oxide flakes, a high carbon purity of ca. 98.3% for G/SWCNT hybrids was achieved when the mole ratio of Fe–Al is 0.05:1. The size and density of Fe nanoparticles decorated in the as-obtained G/SWCNT hybrids depend largely on Fe content in the FeMgAl LDH precursors. Furthermore, the mass ratio of graphene materials to SWCNTs in the as-prepared G/SWCNT hybrids can be well controlled in a range of 0.4–15.1.

© 2013 Elsevier Ltd. All rights reserved.

## 1. Introduction

The combination of one-dimensional carbon nanotubes (CNTs) and two-dimensional graphene into three-dimensional (3D) graphene/CNT (G/CNT) hybrids is considered as one of the most effective strategies to fabricate advanced carbon nanostructures. Both the theoretical and experimental studies have demonstrated that the 3D G/CNT hybrids are with extraordinary mechanical, electrical, and thermal properties due to their ability to integrate the virtues and enhance the dispersion of both graphene and CNTs [1–3]. Consequently, many efforts are devoted on the extensive applications of G/CNT hybrids, including supercapacitors [4–10], Li-ion batteries

[11–13], Li-S batteries [14], electronic and optical devices [3,12,15–18], and heterogeneous catalysis [19,20]. The G/CNT hybrids afford excellent performance for energy storage, chemical conversion, and information technology. The large scale production of G/CNT hybrids with well controlled structures is the prerequisite for any of their bulk application.

Various methods have been explored for the fabrication of G/CNT hybrids, among which the direct mixing of graphene materials and CNTs is the most initially explored method [1]. After that, other post-synthesis routes, including liquid phase reaction routes [3], hydrothermal process [6], electrophoretic deposition [21], layer-by-layer self-assembly [22,23], and liquid/air interface hybridization [24], are also

\* Corresponding author. Fax: +86 10 6277 2051.

E-mail address: [zhang-qiang@mails.tsinghua.edu.cn](mailto:zhang-qiang@mails.tsinghua.edu.cn) (Q. Zhang).  
0008-6223/\$ - see front matter © 2013 Elsevier Ltd. All rights reserved.  
<http://dx.doi.org/10.1016/j.carbon.2013.10.028>

demonstrated to be effective for the fabrication of G/CNT or graphene oxide (GO)/CNT hybrids. However, these post-synthesis methods are insufficient to construct effective connection especially for covalent C–C bonding between graphene layers and CNTs in the hybrids, which significantly limits their performance during the potential applications. Besides, it is difficult to scale up the fabrication of G/CNT hybrids by post-synthesis methods due to the tedious processes. In contrast, the direct growth of G/CNT hybrids through chemical vapor deposition (CVD) is more attractive due to its possibility to provide the covalent C–C bonding between graphene layers and CNTs and the easiness to be scaled up. The most direct and simple idea is to grow CNTs on the surface of GO or reduced GO coated by catalyst nanoparticles (NPs) [4,11,13]. However, the as-grown CNTs in such G/CNT hybrids were always with poor graphitization degree due to the high solubility of catalyst NPs in GO or reduced GO [25]. Besides, the graphene materials in the as-fabricated hybrids was also with a low quality due to the high defect density in GO and reduced GO. These facts dramatically hindered the performance of the as-fabricated G/CNT hybrids during their applications. In order to improve the quality of CNTs, the assistance of  $\text{Al}_2\text{O}_3$  and  $\text{SiO}_2$  barriers were employed to stabilize the catalyst NPs for CNT growth [5,12]. On the other aspect, *in situ* growth of G/CNT hybrids on Fe catalyst layers coated Cu foil was explored to improve the quality of graphene materials in the hybrids [26,27]. It should be noted that the as-grown CNTs in the previous mentioned publications were always multi-walled CNTs (MWCNTs), which led to a low specific surface area (SSA) of the as-fabricated G/CNT hybrids and thus limited their performance related to the surface/interface of G/CNT hybrids.

Compared with MWCNTs, single-walled CNTs (SWCNTs) are with much better intrinsic properties due to their smaller diameter, larger SSA, and lower defect density [28]. Therefore, G/SWCNT hybrids are expected to be with much improved performance compared to G/MWCNT hybrids. Recently, a mixed catalyst of MgO and Fe/MgO was used to achieve the one-step synthesis of G/SWCNT hybrids through CVD, in which MgO served as the template for the growth of graphene materials and Fe/MgO served as the catalyst for the growth of SWCNTs [29]. Similarly, a mixture of NiO and  $\text{Y}_2\text{O}_3$  was adopted to achieve the one-step synthesis of G/SWCNT hybrids by arc-discharge method, in which the oversaturated metal carbon liquid alloy catalyzed the growth of SWCNTs and the evaporation of graphite under  $\text{H}_2$  atmosphere led to the formation of graphene materials [7]. These *in situ* mixing methods can effectively enhance the dispersion of both graphene materials and SWCNTs, and the as-fabricated G/SWCNT hybrids were demonstrated to be with a high SSA and exhibited excellent performance for supercapacitors. However, the covalent C–C bonding between graphene layers and SWCNTs, which is of paramount importance for G/SWCNT hybrids, is impossible to be achieved by such *in situ* mixing methods. The key issue for the *in situ* growth of G/SWCNT hybrids lies in the stability of catalyst NPs during the deposition of graphene materials and SWCNTs. With the assistance of  $\text{Al}_2\text{O}_3$  layer, the Tour group reported the fabrication of G/SWCNT hybrids on Fe catalyst layer coated Cu foil [10]. The covalent C–C bonding between graphene layers

and SWCNTs in the as-fabricated G/SWCNT hybrids was demonstrated and a high surface area of over  $2000 \text{ m}^2/\text{g}$  was achieved, which led to the excellent performance of such G/SWCNT hybrids as electrode materials for supercapacitors. However, the complicated synthesis process hinders the mass production of this kind of G/SWCNT hybrids. On the other hand, considering the extraordinary thermal stability of metal NPs derived from layered double hydroxides (LDHs) [30–32], we reported the successful *in situ* growth of G/SWCNT hybrids through high-temperature CVD using LDHs as the catalyst precursors [8,14] and suggested the covalent C–C bonding between graphene layers and SWCNTs [14]. Both FeMgAl and CoMgAl LDHs were demonstrated to be effective for the fabrication of such G/SWCNT hybrids, which can serve as excellent electrode materials for supercapacitors and Li–S batteries. Furthermore, the LDHs are also considered promising catalysts for the large scale production of G/SWCNT hybrids due to their easiness in scale up.

Up to now, the fluidized-bed catalytic CVD has been demonstrated to be the most efficient way for the mass production of carbon nanomaterials [33–36]. Large scale production of MWCNTs [37,38], SWCNTs [39], aligned CNTs [40,41], and graphene materials [42] have all been successfully achieved in a fluidized-bed reactor. In our previous reports, we have demonstrated the good fluidization behavior of LDHs due to the formation of aggregates originated from the strong interaction between LDH flakes [43]. This renders the large scale production of high-quality SWCNTs in a fluidized-bed reactor using LDHs as the catalyst precursors. In this contribution, we reported the controllable bulk growth of G/SWCNT hybrids with FeMgAl LDH precursors through high-temperature CVD in a fluidized-bed reactor. The yield and structure of the as-produced G/SWCNT hybrids were well controlled by tuning the Fe content in the LDH precursors.

## 2. Experimental sections

### 2.1. Catalyst preparation

A typical urea assisted co-precipitation reaction was employed to prepare the FeMgAl LDH catalyst precursors.  $\text{Fe}(\text{NO}_3)_3 \cdot 9\text{H}_2\text{O}$ ,  $\text{Mg}(\text{NO}_3)_2 \cdot 6\text{H}_2\text{O}$ ,  $\text{Al}(\text{NO}_3)_3 \cdot 9\text{H}_2\text{O}$ , and urea were dissolved in 250.0 mL of deionized water with  $[\text{Fe}^{3+}] + [\text{Mg}^{2+}] + [\text{Al}^{3+}] = 0.15 \text{ mol/L}$ ,  $n(\text{Mg}):n(\text{Al}) = 2:1$ ,  $[\text{urea}] = 3.0 \text{ mol/L}$ . The molar ratios of Fe–Al were controlled at 0.05, 0.1, 0.2, 0.4, and 0.8. The solution was kept at  $100^\circ\text{C}$  under continuous magnetic stirring for 9 h in a flask (equipped with a reflux condenser) of 500.0 mL under ambient atmosphere. Subsequently, the suspension was maintained at  $94^\circ\text{C}$  for 14 h without stirring. FeMgAl LDHs can be available after filtering, washing, and freeze-drying of the as-obtained suspension. The FeMgAl LDH flakes were recorded as LDH-X, where X is the mole ratio of Fe–Al.

### 2.2. Preparation of the G/SWCNT hybrids

The apparatus used for the preparation of G/SWCNT hybrids in this research is similar with that described in our previous publication [40]. The main body is a fluidized bed reactor made of quartz with an inner diameter of 20 mm and a height

of 500 mm. A sintered porous plate is used as the gas distributor and support for solids at the middle of the reactor. The gas mixture entered the bottom vessel of the reactor and then passed through the gas distributor, the fluidized bed units, and finally flowed out during the reaction. Typically, about 1.0 g FeMgAl LDH flakes was fed into the reactor before the reaction. Then, the quartz fluidized bed reactor was mounted in an electrical tube furnace and heated to 950 °C in Ar atmosphere at a flow rate of 500 mL/min. The LDHs were pushed apart from one another due to the up-flow gas at a sufficient velocity. Once reaching the reaction temperature, the flow rate of Ar was turned down to 100 mL/min and CH<sub>4</sub> (400 mL/min) was introduced into the fluidized bed, starting the growth of G/SWCNT hybrids on the surface of the LDH flakes. Both the LDH catalysts and the products can be smoothly fluidized in the reactor during the whole reaction. After the reaction, the fluidized bed reactor was cooled down to room temperature under Ar atmosphere. The as-grown black powders were then collected and characterized.

The as-grown products were treated by HCl (5.0 mol/L) aqueous solution at 80 °C for 3 h and NaOH (15.0 mol/L) aqueous solution at 150 °C for 6 h subsequently to removed the as-calcined FeMgAl layered double oxide (LDO) flakes. G/SWCNT hybrids with different Fe contents were available after filtering, washing, and freeze-drying. The as-obtained G/SWCNT hybrids were recorded as G/S-X, where X is the mole ratio of Fe–Al in the initial FeMgAl LDH catalyst precursors.

### 2.3. Characterizations

The morphology of the G/SWCNT hybrid samples was characterized using a JSM 7401F scanning electron microscope (SEM) operated at 3.0 kV, and a JEM 2010 high resolution transmission electron microscope (TEM) operated at 120.0 kV. The TEM samples were prepared by dropping several drops of the sample suspension obtained by the sonication of about 5 mg of the as-grown products in ethanol onto TEM grids. X-ray diffraction (XRD) patterns were recorded on a Bruker D8 Advance diffractometer at 40.0 kV and 120 mA with Cu-K $\alpha$  radiation. The thermogravimetric analysis (TGA) was carried out using TGA/DSC STAR system under O<sub>2</sub> or CO<sub>2</sub> atmosphere. The Brunauer–Emmett–Teller (BET) SSA of the samples were measured by N<sub>2</sub> adsorption/desorption at liquid-N<sub>2</sub> temperature using Autosorb-IQ<sub>2</sub>-MP-C system. Before measurements, the sample was degassed at 300 °C until a manifold pressure of 2 mmHg was reached. Energy-dispersive

X-ray spectroscopy (EDXS) analysis was performed using a JEM 2010 apparatus equipped with an Oxford Instrument EDXS with the analytical software INCA. Raman spectra were recorded with He–Ne laser excitation at 633 nm using Horiba Jobin Yvon LabRAM HR800 Raman Spectrometer.

## 3. Results and discussion

A family of FeMgAl LDHs with different Fe contents were prepared to serve as the catalyst precursors for the CVD production of G/SWCNT hybrids, which were named as LDH-X, where X is the designed mole ratio of Fe to Al. The chemical compositions of the as-prepared FeMgAl LDHs were confirmed by EDXS analysis and demonstrated to be in good agreement with their designed value (Table 1). All the as-prepared FeMgAl LDHs exhibit the typical hexagonal flake morphology of LDH flakes with a lateral size of ca. 1  $\mu$ m (Fig. 1a). Powder XRD patterns for the as-synthesized FeMgAl LDHs are shown in Fig. 1b. The sharp features of the intrinsic diffraction peaks ((003), (006), and (009)) strongly suggest that the as-prepared FeMgAl LDH flakes are with good crystallinity.

The production of G/SWCNT hybrids was carried out in a fluidized-bed reactor using the as-prepared FeMgAl LDHs as catalyst precursors. Note that a good fluidization behavior was well maintained during the whole reaction under a gas velocity of 10.8 cm/s [43]. After calcination, FeMgAl LDO catalysts were derived from the LDH precursors by subsequent dehydration, decarbonization and the formation of MgAl<sub>2</sub>O<sub>4</sub> spinel phase (>780 °C). Attributed from Kirkendall diffusion of Mg–Fe and/or Mg–Al diffusion couple, mesopores can be available on the as-calcined LDO flakes. However, the flake morphology was well preserved. With the introduction of methane at 950 °C, the LDO catalysts offered two functions: the lamellar LDO flakes served as templates for the deposition of graphene materials, while the embedded small metal NPs produced by the reduction of LDO flakes catalyzed the formation of SWCNTs. Large graphitic shells rather than MWCNTs were grown on the Fe NPs with a size over 4 nm. As shown in Fig. 2a, the as-obtained black products exhibit the morphology of CNTs interlinked with flakes. The morphologies of the products derived from FeMgAl LDHs with varied Fe contents did not differ a lot, indicating the robust growth of G/SWCNT hybrids on LDO catalysts in a fluidized bed reactor. Fig. 2a–c illustrated the typical SEM and TEM images of the products obtained with LDH-0.1 as the catalyst precursors. Large amount of SWCNTs were efficiently synthesized on the surface of the

**Table 1 – Growth of G/SWCNT hybrids on LDH derived catalysts.**

LDHs	Composition <sup>a</sup> (n(Fe):n(Mg):n(Al))	Formula	Fe content in the LDOs <sup>b</sup> (%)	G/SWCNT hybrids	Yield <sup>c</sup> (g <sub>G/SWCNTs</sub> /g <sub>cat</sub> )
LDH-0.05	0.06:1.9:1	[Mg <sub>0.64</sub> Al <sub>0.34</sub> Fe <sub>0.02</sub> (OH) <sub>2</sub> ][(CO <sub>3</sub> ) <sub>0.18</sub> ]·mH <sub>2</sub> O	2.5	G/S-0.05	0.59
LDH-0.1	0.11:1.8:1	[Mg <sub>0.62</sub> Al <sub>0.34</sub> Fe <sub>0.04</sub> (OH) <sub>2</sub> ][(CO <sub>3</sub> ) <sub>0.19</sub> ]·mH <sub>2</sub> O	4.9	G/S-0.1	0.68
LDH-0.2	0.19:1.9:1	[Mg <sub>0.61</sub> Al <sub>0.32</sub> Fe <sub>0.06</sub> (OH) <sub>2</sub> ][(CO <sub>3</sub> ) <sub>0.19</sub> ]·mH <sub>2</sub> O	7.4	G/S-0.2	0.84
LDH-0.4	0.35:1.9:1	[Mg <sub>0.58</sub> Al <sub>0.31</sub> Fe <sub>0.11</sub> (OH) <sub>2</sub> ][(CO <sub>3</sub> ) <sub>0.21</sub> ]·mH <sub>2</sub> O	12.9	G/S-0.4	0.97
LDH-0.8	0.83:1.6:1	[Mg <sub>0.47</sub> Al <sub>0.29</sub> Fe <sub>0.24</sub> (OH) <sub>2</sub> ][(CO <sub>3</sub> ) <sub>0.27</sub> ]·mH <sub>2</sub> O	25.5	G/S-0.8	0.85

<sup>a</sup> The composition was determined by EDXS analysis.

<sup>b</sup> The Fe content in the LDOs was calculated based on the formula of LDHs.

<sup>c</sup> The yield was determined by TGA results of the G/SWCNT/LDO composites.

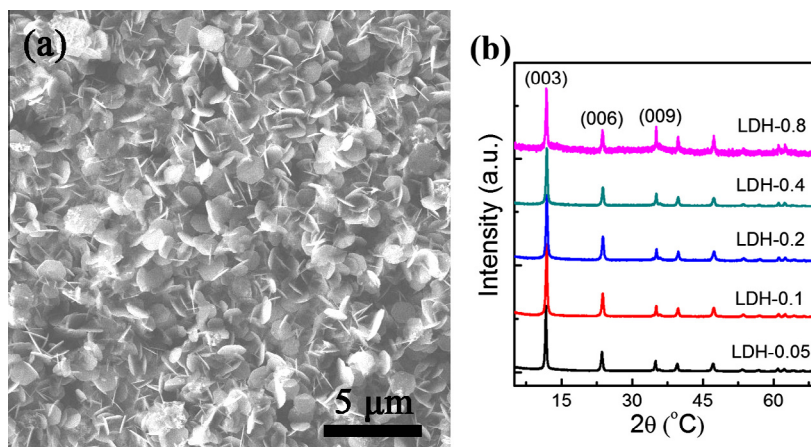


Fig. 1 – (a) SEM image of LDH-0.2 and (b) XRD spectra of the as-prepared FeMgAl LDH catalysts. (A color version of this figure can be viewed online.)

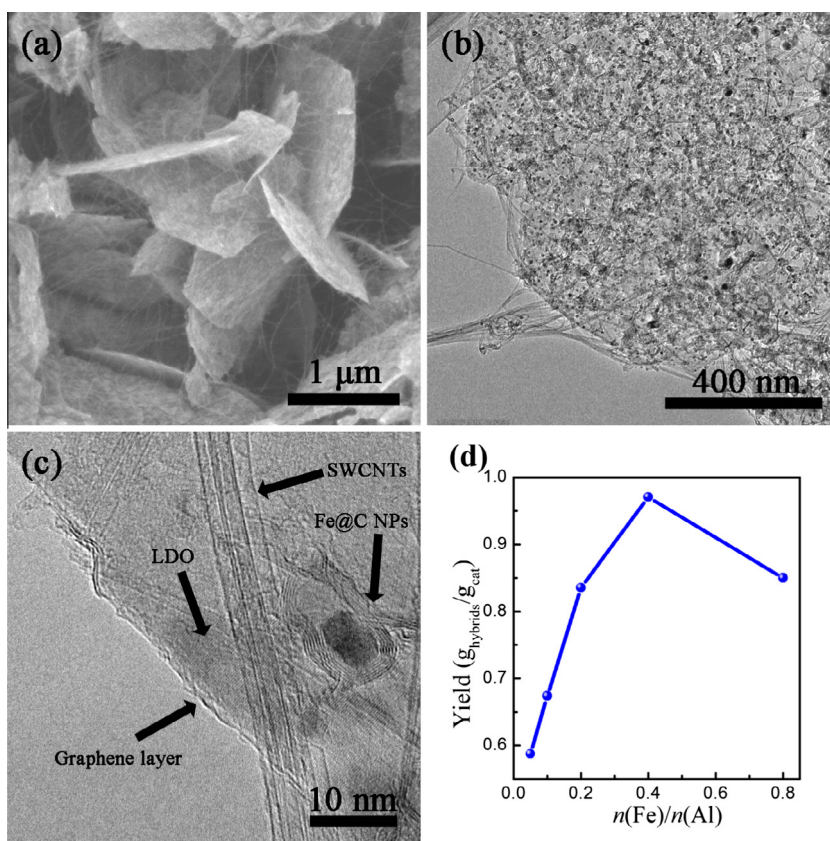
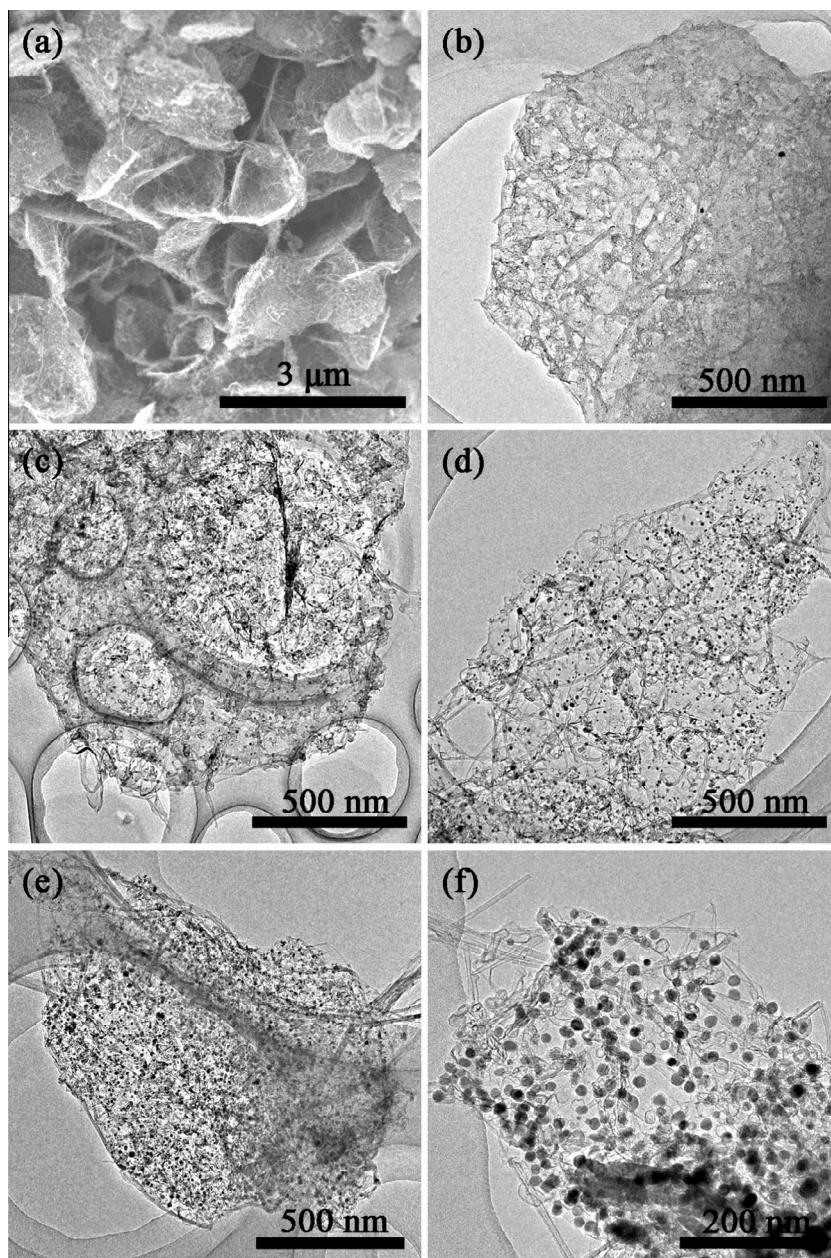


Fig. 2 – (a) SEM, (b) TEM and (c) high-resolution TEM images of the typical morphology of the as-grown G/SWCNT/LDO composites from the FeMgAl LDHs (LDH-0.1); (d) the relationship between the yield of the G/SWCNT hybrids and the designed values of  $n(\text{Fe})/n(\text{Al})$  for the FeMgAl LDH catalysts. (A color version of this figure can be viewed online.)

FeMgAl LDO flakes (Fig. 2a). Few-layer graphene was also observed on the surface of LDO flakes. Besides, the existence of large quantity of graphene materials encapsulated Fe NPs (Fe@C NPs) in the products were demonstrated (Fig. 2c).

The growth of SWCNT is heavily depended on the Fe content in the FeMgAl LDHs [31]. Herein, the yield of G/SWCNT hybrids derived from FeMgAl LDHs differed a lot with the

increasing Fe content (Fig. 2d and Table 1). When LDH-0.05 served as the catalyst precursor, a yield of  $0.59 \text{ g}_{\text{G/SWCNT}}/\text{g}_{\text{cat}}$  was achieved, which was much higher than that when only SWCNTs were obtained with the same catalyst ( $0.17 \text{ g}_{\text{SWCNT}}/\text{g}_{\text{cat}}$ ) at a lower temperature of  $900^\circ\text{C}$  [31]. This was attributed to the efficient deposition of graphene materials on the LDO flakes in addition to the growth of SWCNTs during the



**Fig. 3 – (a) SEM image of the typical morphology of the as-obtained G/SWCNT hybrids; TEM images of the morphology of the as-obtained G/SWCNT hybrids: (b) G/S-0.05, (c) G/S-0.1, (d) G/S-0.2, (e) G/S-0.4, (f) G/S-0.8.**

high-temperature CVD. With the increasing Fe content, more G/SWCNT hybrids were available. A high yield of  $0.97 \text{ g}_{\text{G/SWCNT}}/\text{g}_{\text{cat}}$  was achieved when using LDH-0.4 as the catalyst precursor. This phenomenon is considered to be mainly contributed by two facts: (i) the increasing Fe content in the FeMgAl LDHs leads to the increased amount of the as-grown SWCNTs from LDHs; (ii) the increasing Fe content also results in the increased size of the as-produced Fe NPs from FeMgAl LDHs, which intend to form Fe@C NPs, leading to the increased amount of the as-deposited graphene materials on Fe NPs. However, the enlarged size of Fe NPs significantly hinders the growth of SWCNTs [31]. As a result, a small drop of the yield of G/SWCNT hybrids was observed when the Fe content was too high (Fig. 2d).

The FeMgAl LDO flakes in the products can be removed by subsequent acid and alkali treatments, and the as-obtained G/SWCNT hybrids were denoted as G/S-X, where X is the designed mole ratio of Fe–Al in the FeMgAl LDH precursors (Table 1). There is no significant difference on the morphology of the as-obtained G/SWCNT hybrids from FeMgAl LDHs with increasing Fe content, and they all exhibit the similar morphology of SWCNTs interlinked with graphene layers (Fig. 3). The stacking of graphene layers and the aggregation of SWCNTs are successfully prevented due to their hybridization. The TEM images shown in Fig. 3b–f illustrate the existence of more Fe@C NPs in the as-obtained G/SWCNT hybrids with the increasing Fe content. For G/S-0.05, only a few Fe@C NPs with a small size can be observed. With the

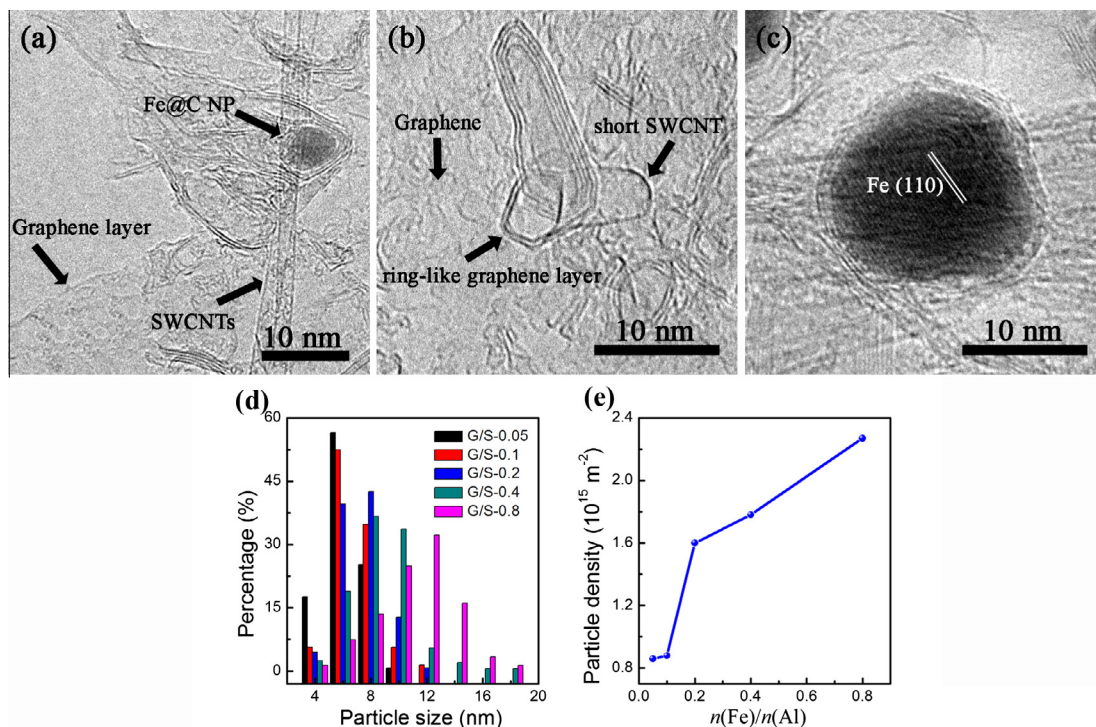


**Fig. 4** – High resolution TEM images of the typical morphology of (a) the G/SWCNT hybrids, (b) the interface between graphene and SWCNT, and (c) the Fe@C NP from G/S-0.4; (d) size distribution and (e) density of Fe NPs in the as-obtained G/SWCNT hybrids from FeMgAl LDHs with different Fe contents, in which the  $n(\text{Fe})/n(\text{Al})$  is the designed molar ratio of Fe–Al for the LDH precursors. (A color version of this figure can be viewed online.)

increasing Fe content, both the size and density of the Fe@C NPs in the as-obtained G/SWCNT hybrids increase a lot. Especially, large amount of Fe@C NPs with a large size around 12 nm and uniform dispersion can be easily observed for G/S-0.8. The few-layer graphene is much easier to be torn up by sonication for the G/SWCNT hybrids derived from high Fe-loading LDHs, indicating the existence of large amount of Fe@C NPs plays a negative effect on the quality of few-layer graphene (Fig. 3d–f). Apparently, the graphene materials deposited on the LDO flakes are more defective than those grown on metal substrate by CVD, but they are expected with better electrical conductivity than GO and reduced GO, which plays an important role in the good electrochemical performance of the G/SWCNT hybrids derived from LDHs [8,14].

Fig. 4a shows the typical high resolution TEM images of the G/SWCNT hybrids, which are composed of few-layer graphene, SWCNTs, and Fe@C NPs. The morphology of the interface between graphene and SWCNT is shown in Fig. 4b, in which the whole background is the graphene. It is noticed that a ring-like structure composed of graphene layer can be observed at the root of a short SWCNT. This is a common phenomenon for the G/SWCNT hybrids derived from LDHs [8,14], but it cannot be found when only SWCNTs are grown from the LDHs [31]. It has been demonstrated that the existence of such ring-like structure is a characteristic property for covalent C–C bonds between SWCNTs and graphene layers, which implies that the SWCNTs are open-ended [10]. Therefore, the as-obtained G/SWCNT hybrids from LDHs are probably with a covalent C–C bonding between the graphene layers

and SWCNTs. The complete encapsulation of Fe NPs by graphene materials effectively prevents the attacking of Fe atoms by acid molecular during the acid treatment, which makes the Fe@C NPs difficult to be removed by the typical acid treatment (Fig. 4c). The uniform dispersion of Fe@C NPs in the G/SWCNT hybrids renders the possibility to carry out the statistical analysis of their size and density distribution, which are shown in Fig. 4d and e. For G/S-0.05, the size of Fe NPs is mainly distributed in a range of 4.0–8.0 nm with a mean size of 6.2 nm. The size of Fe NPs in the as-prepared G/SWCNT hybrids increases gradually with the increasing Fe content in the original LDH precursors, as shown in Fig. 4d. The mean size of Fe NPs in G/S-0.1 is 6.8 nm, which further increased to 7.2, 8.6, and 14.8 nm for G/S-0.2, 0.4, and 0.8, respectively. Furthermore, the density of Fe NPs also increased from  $0.86 \times 10^{15} \text{ m}^{-2}$  for G/S-0.05 to  $2.27 \times 10^{15} \text{ m}^{-2}$  for G/S-0.8 (Fig. 4e). Consequently, Fe NPs with well controlled size and density encapsulated by graphene materials and uniformly distributed on the G/SWCNT hybrids can be obtained when using different Fe-containing FeMgAl LDHs as the catalyst precursors.

The increasing size and density of Fe NPs in the as-purified G/SWCNT hybrids lead to their decreased purity and thermal stability (Fig. 5a and b, Table 2). TGA results shown in Fig. 5a reveal that G/SWCNT hybrids with a high carbon purity of 98.3% are available after the preliminary acid and alkali treatment for LDH-0.05. However, the purity of G/SWCNT hybrids decreased significantly to 81.1% for G/S-0.8, indicating more Fe NPs are preserved in the form of Fe@C NPs with the

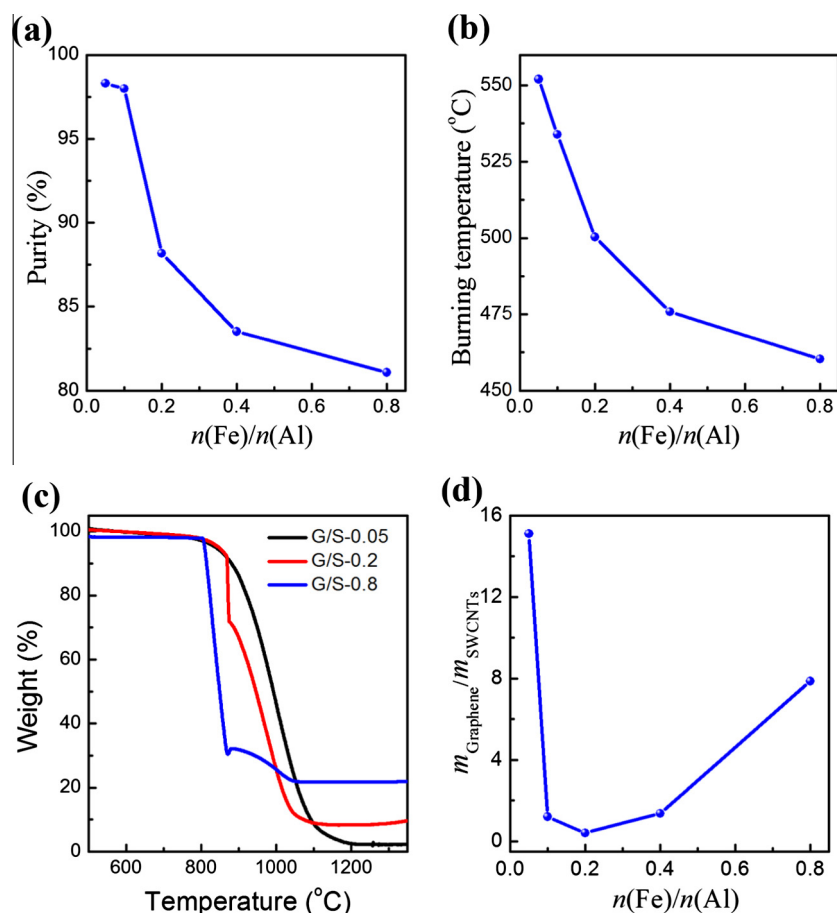


**Fig. 5** – (a) The purities and (b) burning temperatures of the as-obtained G/SWCNT hybrids from FeMgAl LDHs with different Fe contents; (c) typical TGA curves of the as-obtained G/SWCNT hybrids from FeMgAl LDHs with different Fe contents under  $\text{CO}_2$  atmosphere; (d) the mass ratios of graphene materials to SWCNTs in the as-obtained G/SWCNT hybrids from FeMgAl LDHs with different Fe contents. The  $n(\text{Fe})/n(\text{Al})$  is the designed molar ratio of Fe–Al for the LDH precursors. (A color version of this figure can be viewed online.)

**Table 2** – The summary of structures and properties of the as-obtained G/SWCNT hybrids.

G/SWCNT hybrids	Purity (%)	Burning temperature (°C)	$m_{\text{Graphene}}/m_{\text{SWCNTs}}$	$I_D/I_G$	$\text{SSA}_{\text{G/SWCNTs}}$ ( $\text{m}^2/\text{g}$ )	Pore volume ( $\text{cm}^3/\text{g}$ )
G/S-0.05	98.3	552.0	15.1	0.11	696.3	1.69
G/S-0.1	98.0	534.0	1.2	0.16	577.9	1.84
G/S-0.2	88.2	500.3	0.4	0.12	517.0	1.79
G/S-0.4	83.0	475.8	1.4	0.26	488.4	1.68
G/S-0.8	81.1	460.4	7.9	0.47	229.5	0.93

increasing Fe content for FeMgAl LDHs (Table 2). The strong interaction between C and Fe in the carbon encapsulated Fe NPs could efficiently promote the reaction activity of carbon atoms, which renders such nanostructure a good catalyst for oxidation reduction reaction [44]. Herein, during the TGA measurement, the Fe NPs catalyze the oxidation of nanocarbon to CO and  $\text{CO}_2$  [45,46]. Consequently, a much better oxidation activity is expected for G/SWCNT hybrids with increasing Fe content. As shown in Fig. 5b and Table 2, the burning temperature for G/S-0.05 was around 550 °C in oxygen atmosphere, which decreased dramatically with the increasing Fe content. A low burning temperature around 460 °C was

determined for G/S-0.8. In spite of Fe content, the mass ratio of graphene materials to SWCNTs ( $m_{\text{graphene}}/m_{\text{SWCNTs}}$ ) in the G/SWCNT hybrids also plays an important role in their properties. Herein, the mass ratios of graphene materials to SWCNTs in the G/SWCNT hybrids were characterized by TGA under  $\text{CO}_2$  atmosphere. As shown in Fig. 5c, all the TGA curves under  $\text{CO}_2$  atmosphere for G/SWCNT hybrids with different Fe contents exhibit two significant weight loss regions. It has been demonstrated by TEM observation that the first weight loss regions correspond to the oxidation of both the graphene materials coating on the Fe NPs and the lateral few-layer graphene deposited on LDO flakes due to

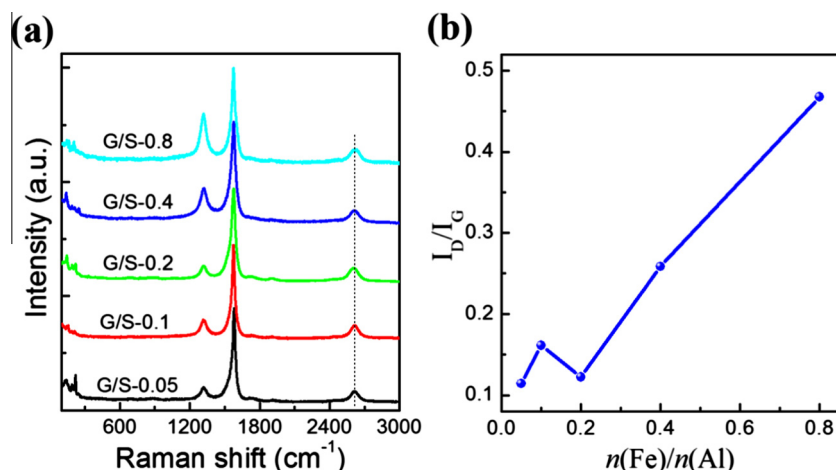


**Fig. 6 – (a) Raman spectra and (b)  $I_D/I_G$  values of the as-obtained G/SWCNT hybrids from FeMgAl LDHs with different Fe contents, in which the  $n(\text{Fe})/n(\text{Al})$  is the designed molar ratio of Fe–Al for the LDH precursors. (A color version of this figure can be viewed online.)**

the catalyzing effect and migration of the Fe NPs during the  $\text{CO}_2$ -oxidation, and the second weight loss regions correspond to the oxidation of SWCNTs [14]. Note that the graphene materials encapsulated on Fe NPs devote to the total mass of graphene materials in the G/SWCNT hybrids in this  $\text{CO}_2$ -TGA method [14]. The small weight increase observed at the connection between the two oxidation regions in the TGA curve under  $\text{CO}_2$  atmosphere for G/SWCNT hybrids with a high Fe content (G/S-0.8) can be attributed to the oxidation of Fe after the complete removal of the encapsulated graphene materials. A high  $m_{\text{graphene}}/m_{\text{SWCNTs}}$  value of 15.1 was measured for G/S-0.05, indicating few SWCNTs can be synthesized when the Fe content was too low for FeMgAl LDHs (Fig. 5d, Table 2). The  $m_{\text{graphene}}/m_{\text{SWCNTs}}$  value decreased a lot with the increasing Fe content in the LDH precursors, which reached the lowest value of 0.4 for G/S-0.2 (Table 2). When the Fe content further increased, the growth of SWCNTs was significantly hindered due to the increased size of Fe catalyst NPs, which also led to the increasing amount of Fe@C NPs [31]. As a result, the  $m_{\text{graphene}}/m_{\text{SWCNTs}}$  value increased to 1.4 for G/S-0.4 and further increased to 7.9 for G/S-0.8 (Fig. 5d, Table 2).

Fig. 6a shows the Raman spectra for the as-prepared G/SWCNT hybrids with different Fe contents. Obvious radial breathing mode peaks were observed for all the samples, indicating the existence of large amount of SWCNTs. The value of  $I_D/I_G$  (intensity ratio of D band ( $\sim 1318 \text{ cm}^{-1}$ ) to G band ( $\sim 1575 \text{ cm}^{-1}$ )) was measured as 0.11 for G/S-0.05, indicating the good graphitization degree for the as-prepared G/SWCNT hybrids. The  $I_D/I_G$  value gradually increased with increasing Fe content, indicating the decreased graphitization degree for the G/SWCNT hybrids obtained from high Fe-contained FeMgAl LDHs (Table 2). This can be attributed to the formation of large amount of Fe@C NPs.  $\text{N}_2$ -adsorption analysis was carried out to characterize the BET SSA and porous structure of the as-prepared G/SWCNT hybrids. A high SSA of  $696.3 \text{ m}^2/\text{g}$  and a total pore volume of  $1.69 \text{ cm}^3/\text{g}$  were determined for G/S-0.05, both of which decreased a lot with the increasing Fe content (Table 2). For instance, a much lower SSA value

of  $229.5 \text{ m}^2/\text{g}$  was obtained for G/S-0.8, the total pore volume of which decreased to  $0.93 \text{ cm}^3/\text{g}$  due to the existence of large amount of Fe@C NPs.

Finally, it should be noted that there are still metal catalyst residuals in the as-produced G/SWCNT hybrids. The metal residuals were completely encapsulated by the graphitic shells. On one aspect, the metal residuals render novel reactivity for selective oxidation, reduction, and dehydrogenation, which is highly required to tune the interfacial chemistry for fuel cells [44] as well as heterogeneous catalysis [47]. On the other aspect, the metal residuals may be leached from the hybrids during charge–discharge processes at a wide voltage window in organic and/or ionic liquid electrolyte for supercapacitor or battery applications, which results in their poor stability. Therefore, G/SWCNT hybrids with a very high carbon purity are highly required. Enlightened by the catalytic gasification of carbon by the metal residuals, the use of weak oxidation atmospheres to open the graphitic shells and expose the metal NPs can be realized by mediating the selection of oxidants and related operation windows. Recently, ultra-high purity of SWCNT with a carbon content of 99.5 wt% can be achieved by a  $\text{CO}_2$ -assisted purification [48]. It has also been demonstrated that Fe NPs in the G/SWCNT hybrids can also be effectively removed by such  $\text{CO}_2$ -assisted purification to improve the purity of G/SWCNT hybrids [14]. Further investigation on the ultra-high purity G/SWCNT hybrids and their intrinsic physical and chemical properties, as well as the relationships among the G/SWCNT structure, ratio, property, and bulk applications are still being carried out.

#### 4. Conclusions

Efficient growth of G/SWCNT hybrids with well controlled structure was achieved by fluidized-bed CVD at  $950 \text{ }^\circ\text{C}$  on FeMgAl LDH derived catalysts. Fe content in the FeMgAl LDHs was varied to achieve the structure control for the as-obtained G/SWCNT hybrids. The yield of the as-grown G/SWCNT hybrids varied from 0.59 to  $0.97 \text{ g}_{\text{G/SWCNTs}}/\text{g}_{\text{cat}}$  with different Fe contents in the LDH flakes. G/SWCNT hybrids

exhibiting the morphology of SWCNTs interlinked with graphene layers and contained by Fe@C NPs were obtained after the removal of FeMgAl LDO flakes. The size of Fe NPs in the as-purified G/SWCNT hybrids can be well controlled in a range of 3.0–18.0 nm with their density in a range of  $0.9\text{--}2.3 \times 10^{15} \text{ m}^{-2}$  by adjusting the Fe content in the LDH precursors. A high carbon purity of 98.3% for the G/SWCNT hybrids can be achieved with the low Fe-containing LDHs, and a high Fe proportion of ca. 18.9% in the form of Fe@C NPs can be obtained with the high Fe-containing LDHs. The mass ratio of graphene materials to SWCNTs in the G/SWCNT hybrids was controllable ranging from 0.4 to 15.1. The SSA of the as-purified G/SWCNT hybrids decreased from ca. 700 to 200  $\text{m}^2/\text{g}$  with the increasing Fe content and their total pore volume decreased from 1.60 to 0.93  $\text{cm}^3/\text{g}$ . The production of G/SWCNT hybrids with well controlled structure in the fluidized-bed reactor is easy to be scaled up for their large scale applications in the area of energy storage and conversion, composites, and catalysis.

## Acknowledgements

This work was supported by National Basic Research Program of China (973 Program 2011CB932602) and Natural Scientific Foundation of China (No. 21306102).

## REFERENCES

- [1] Cai D, Song M, Xu C. Highly conductive carbon-nanotube/graphite-oxide hybrid films. *Adv Mater* 2008;20(9):1706–9.
- [2] Xu L, Wei N, Zheng Y, Fan Z, Wang HQ, Zheng JC. Graphene-nanotube 3D networks: intriguing thermal and mechanical properties. *J Mater Chem* 2011;22(4):1435–44.
- [3] Tung VC, Chen LM, Allen MJ, Wassei JK, Nelson K, Kaner RB, et al. Low-temperature solution processing of graphene-carbon nanotube hybrid materials for high-performance transparent conductors. *Nano Lett* 2009;9(5):1949–55.
- [4] Fan Z, Yan J, Zhi L, Zhang Q, Wei T, Feng J, et al. A three-dimensional carbon nanotube/graphene sandwich and its application as electrode in supercapacitors. *Adv Mater* 2010;22(33):3723–8.
- [5] Du F, Yu D, Dai L, Ganguli S, Varshney V, Roy AK. Preparation of tunable 3D pillared carbon nanotube-graphene networks for high-performance capacitance. *Chem Mater* 2011;23(21):4810–6.
- [6] Wang Y, Wu Y, Huang Y, Zhang F, Yang X, Ma Y, et al. Preventing graphene sheets from restacking for high-capacitance performance. *J Phys Chem C* 2011;115(46):23192–7.
- [7] Wu YP, Zhang TF, Zhang F, Wang Y, Ma YF, Huang Y, et al. *In situ* synthesis of graphene/single-walled carbon nanotube hybrid material by arc-discharge and its application in supercapacitors. *Nano Energy* 2012;1(6):820–7.
- [8] Zhao MQ, Zhang Q, Huang JQ, Tian GL, Chen TC, Qian WZ, et al. Towards high purity graphene/single-walled carbon nanotube hybrids with improved electrochemical capacitive performance. *Carbon* 2013;54:403–11.
- [9] Lin J, Zhang C, Yan Z, Zhu Y, Peng Z, Hauge RH, et al. 3-dimensional graphene carbon nanotube carpet-based microsupercapacitors with high electrochemical performance. *Nano Lett* 2013;13(1):72–8.
- [10] Zhu Y, Li L, Zhang C, Casillas G, Sun Z, Yan Z, et al. A seamless three-dimensional carbon nanotube graphene hybrid material. *Nat Commun* 2012;3:1225.
- [11] Fan ZJ, Yan J, Wei T, Ning GQ, Zhi LJ, Liu JC, et al. Nanographene-constructed carbon nanofibers grown on graphene sheets by chemical vapor deposition: high-performance anode materials for lithium ion batteries. *ACS Nano* 2011;5(4):2787–94.
- [12] Li S, Luo Y, Lv W, Yu W, Wu S, Hou P, et al. Vertically aligned carbon nanotubes grown on graphene paper as electrodes in lithium-ion batteries and dye-sensitized solar cells. *Adv Energy Mater* 2011;1(4):486–90.
- [13] Chen S, Chen P, Wang Y. Carbon nanotubes grown *in situ* on graphene nanosheets as superior anodes for Li-ion batteries. *Nanoscale* 2011;3(10):4323–9.
- [14] Zhao MQ, Liu XF, Zhang Q, Tian GL, Huang JQ, Zhu W, et al. Graphene/single-walled carbon nanotube hybrids: one-step catalytic growth and applications for high-rate Li-S batteries. *ACS Nano* 2012;6(12):10759–69.
- [15] Li B, Cao X, Ong HG, Cheah JW, Zhou X, Yin Z, et al. All-carbon electronic devices fabricated by directly grown single-walled carbon nanotubes on reduced graphene oxide electrodes. *Adv Mater* 2010;22(28):3058–61.
- [16] Kim UJ, Lee IH, Bae JJ, Lee S, Han GH, Chae SJ, et al. Graphene/carbon nanotube hybrid-based transparent 2D optical array. *Adv Mater* 2011;23(33):3809–14.
- [17] Dong X, Xing G, Chan-Park MB, Shi W, Xiao N, Wang J, et al. The formation of a carbon nanotube-graphene oxide core-shell structure and its possible applications. *Carbon* 2011;49(15):5071–8.
- [18] Yen MY, Hsiao MC, Liao SH, Liu PI, Tsai HM, Ma C, et al. Preparation of graphene/multi-walled carbon nanotube hybrid and its use as photoanodes of dye-sensitized solar cells. *Carbon* 2011;49(11):3597–606.
- [19] Lv RT, Cui T, Jun MS, Zhang Q, Cao A, Su DS, et al. Open-ended, N-doped carbon nanotube-graphene hybrid nanostructures as high-performance catalyst support. *Adv Funct Mater* 2011;21(5):999–1006.
- [20] Li Y, Zhou W, Wang H, Xie L, Liang Y, Wei F, et al. An oxygen reduction electrocatalyst based on carbon nanotube-graphene complexes. *Nat Nanotechnol* 2012;7(6):394–400.
- [21] Bon SB, Valentini L, Kenny JM, Peponi L, Verdejo R, Lopez-Manchado MA. Electrodeposition of transparent and conducting graphene/carbon nanotube thin films. *Phys Status Solidi A* 2010;207(11):2461–6.
- [22] Byon HR, Lee SW, Chen S, Hammond PT, Shao-Horn Y. Thin films of carbon nanotubes and chemically reduced graphenes for electrochemical micro-capacitors. *Carbon* 2011;49(2):457–67.
- [23] Hong TK, Lee DW, Choi HJ, Shin HS, Kim BS. Transparent, flexible conducting hybrid multi layer thin films of multiwalled carbon nanotubes with graphene nanosheets. *ACS Nano* 2010;4(7):3861–8.
- [24] Shao JJ, Lv W, Guo Q, Zhang C, Xu Q, Yang QH, et al. Hybridization of graphene oxide and carbon nanotubes at the liquid/air interface. *Chem Commun* 2012;48(31):3706–8.
- [25] Rinaldi A, Tessonnier J-P, Schuster ME, Blume R, Girgsdies F, Zhang Q, et al. Dissolved carbon controls the initial stages of nanocarbon growth. *Angew Chem Int Ed* 2011;50(14):3313–7.
- [26] Paul RK, Ghazinejad M, Penchev M, Lin J, Ozkan M, Ozkan CS. Synthesis of a pillared graphene nanostructure: a counterpart of three-dimensional carbon architectures. *Small* 2010;6(20):2309–13.
- [27] Lee DH, Kim JE, Han TH, Hwang JW, Jeon S, Choi SY, et al. Versatile carbon hybrid films composed of vertical carbon nanotubes grown on mechanically compliant graphene films. *Adv Mater* 2010;22(11):1247–52.

- [28] Zhou WY, Bai XD, Wang EG, Xie SS. Synthesis, structure, and properties of single-walled carbon nanotubes. *Adv Mater* 2009;21(45):4565–83.
- [29] Zhu X, Ning G, Fan Z, Gao J, Xu C, Qian W, et al. One-step synthesis of a graphene–carbon nanotube hybrid decorated by magnetic nanoparticles. *Carbon* 2012;50(8):2764–71.
- [30] Zhao MQ, Tian GL, Zhang Q, Huang JQ, Nie JQ, Wei F. Preferential growth of short aligned, metallic-rich single-walled carbon nanotubes from perpendicular layered double hydroxide film. *Nanoscale* 2012;4(7):2470–7.
- [31] Zhao MQ, Zhang Q, Jia XL, Huang JQ, Zhang YH, Wei F. Hierarchical composites of single/double-walled carbon nanotubes interlinked flakes from direct carbon deposition on layered double hydroxides. *Adv Funct Mater* 2010;20(4):677–85.
- [32] Zhao MQ, Zhang Q, Zhang W, Huang JQ, Zhang Y, Su DS, et al. Embedded high density metal nanoparticles with extraordinary thermal stability derived from guest–host mediated layered double hydroxides. *J Am Chem Soc* 2010;132(42):14739–41.
- [33] Danafar F, Fakhru'l-Razi A, Salleh MAM, Biak DRA. Fluidized bed catalytic chemical vapor deposition synthesis of carbon nanotubes – a review. *Chem Eng J* 2009;155(1–2):37–48.
- [34] See CH, Harris AT. A review of carbon nanotube synthesis via fluidized-bed chemical vapor deposition. *Ind Eng Chem Res* 2007;46(4):997–1012.
- [35] Wei F, Zhang Q, Qian WZ, Yu H, Wang Y, Luo GH, et al. The mass production of carbon nanotubes using a nano-agglomerate fluidized bed reactor: a multiscale space-time analysis. *Powder Technol* 2008;183(1):10–20.
- [36] Zhang Q, Huang JQ, Zhao MQ, Qian WZ, Wei F. Carbon nanotube mass production: principles and processes. *ChemSusChem* 2011;4(7):864–89.
- [37] Wang Y, Wei F, Luo GH, Yu H, Gu GS. The large-scale production of carbon nanotubes in a nano-agglomerate fluidized-bed reactor. *Chem Phys Lett* 2002;364(5–6):568–72.
- [38] Zhang Q, Yu H, Liu Y, Qian WZ, Wang Y, Luo GH, et al. Few walled carbon nanotube production in large-scale by nano-agglomerate fluidized-bed process. *Nano* 2008;3(1):45–50.
- [39] Li Y, Zhang XB, Shen LH, Luo JH, Tao XY, Liu F, et al. Controlling the diameters in large-scale synthesis of single-walled carbon nanotubes by catalytic decomposition of CH<sub>4</sub>. *Chem Phys Lett* 2004;398(1–3):276–82.
- [40] Zhang Q, Zhao MQ, Huang JQ, Liu Y, Wang Y, Qian WZ, et al. Vertically aligned carbon nanotube arrays grown on a lamellar catalyst by fluidized bed catalytic chemical vapor deposition. *Carbon* 2009;47(11):2600–10.
- [41] Zhang Q, Zhao MQ, Huang JQ, Nie JQ, Wei F. Mass production of aligned carbon nanotube arrays grown on clay by fluidized bed catalytic chemical vapor deposition. *Carbon* 2010;48(4):1196–209.
- [42] Ning G, Fan Z, Wang G, Gao J, Qian W, Wei F. Gram-scale synthesis of nanomesh graphene with high surface area and its application in supercapacitor electrodes. *Chem Commun* 2011;47(21):5976–8.
- [43] Zhao MQ, Zhang Q, Huang JQ, Nie JQ, Wei F. Layered double hydroxides as catalysts for the efficient growth of high quality single-walled carbon nanotubes in a fluidized bed reactor. *Carbon* 2010;48(11):3260–70.
- [44] Deng DH, Yu L, Chen X, Wang G, Jin L, Pan XL, et al. Iron encapsulated within pod-like carbon nanotubes for oxygen reduction reaction. *Angew Chem Int Ed* 2013;52(1):371–5.
- [45] Marsh H, Rodriguez-Reinoso F. *Activated carbon*. Amsterdam: Elsevier; 2006. p. 243–321.
- [46] Huang JQ, Zhang Q, Zhao MQ, Wei F. The release of free standing vertically-aligned carbon nanotube arrays from a substrate using CO<sub>2</sub> oxidation. *Carbon* 2010;48(5):1441–50.
- [47] Zhang J, Comotti M, Schuth F, Schlögl R, Su DS. Commercial Fe- or Co-containing carbon nanotubes as catalysts for NH<sub>3</sub> decomposition. *Chem Commun* 2007;19:1916–8.
- [48] Chen TC, Zhao MQ, Zhang Q, Tian GL, Huang JQ, Wei F. In situ monitoring the role of working metal catalyst nanoparticles for ultrahigh purity single-walled carbon nanotubes. *Adv Funct Mater* 2013;23(40):5066–73.